Scanning Electron Microscopy

Volume 1982
Number 1 *1982*

Article 28

1982

Monte Carlo Simulation of Spatial Resolution Limits in Electron Beam Lithography

David F. Kyser
Philips Research Laboratories Sunnyvale Signetics Corporation

Electron Beam Interactions With Solids (Pp. 331-342)
SEM, Inc., AMF O'Hare (Chicago), IL 60666, U.S.A.

MONTE CARLO SIMULATION OF SPATIAL RESOLUTION LIMITS IN ELECTRON BEAM LITHOGRAPHY

DAVID F. KYSER
Philips Research Laboratories Sunnyvale
Signetics Corporation
Sunnyvale, California 94086

Phone No.: (408) 746-1452

ABSTRACT

Computer simulation of high energy primary electron scattering and subsequent generation of "fast" secondary electrons in thin film targets is demonstrated with Monte Carlo techniques. The hybrid model of Murata et al. (1981) is utilized to calculate the generation and subsequent spatial trajectory of each secondary electron in the target. The 3-dimensional spatial distribution of energy dissipation by such "fast" secondary electrons is shown to be the fundamental resolution limit for electron beam lithography with high-voltage beams (100 keV) and thin film polymer targets. The dependence of resolution on beam voltage and film thickness is presented, and quantitative comparison is made between these new Monte Carlo calculations and the limited amount of experimental data available in the scientific literature.

Keywords: Monte Carlo calculation, electron scattering, electron energy deposition, electron beam lithography, secondary electron production, spatial resolution limits, nanolithography, energy density contours, development contours.

I. INTRODUCTION

The interaction of an electron beam with polymeric resist films produces a spatial distribution of energy deposition which causes the so-called proximity effect in electron beam lithography. The quantitative characteristics of the spatial distribution are determined by parameters such as electron beam voltage, electron dose, film thickness, and substrate material. The local magnitude of energy density absorbed (eV/cm^3) is generally linear with electron exposure for the conditions encountered in electron beam lithography. This is to be contrasted with optical exposure of photoresist materials, where there are so-called bleaching effects which result in local non-linear deposition of energy with photon exposure.

The solubility rate of polymeric resist materials is generally non-linear with energy absorbed, and so the actual lithographic performance of a resist is determined both by the spatial distribution of energy deposition (latent image) and the solubility rate curve of the particular resist-solvent utilized. The time-evolution of the pattern etched in the resist film (developed image) is important to understand and control for advances in microlithography and microstructure technology. The ultimate resolution, or spatial distribution of the latent image in electron lithography, is generally agreed to be determined by the production and interaction of secondary electrons within the resist film, and not by the incident primary electrons.

Many theoretical models have been utilized to calculate the spatial distribution of energy deposition by an electron beam in solid targets, including closed-form analytical models and statistical Monte-Carlo models of electron scattering and energy loss. In most cases, only the incident primary electron scattering is accounted for. However, when a primary electron enters the target, it transfers its kinetic energy to atomic electrons by ionization and excitation which results in fast secondary electron production within the resist film. These fast secondary electrons are produced with a kinetic energy distribution from near zero up to one half of the primary electron energy. In a recent paper by Murata et al. (1981) the cross-section for fast secondary electron production was utilized within a hybrid Monte Carlo calculation of electron scattering to predict the quantitative effects of such electrons on spatial resolution limits. The results obtained for 20 keV

exposure of 0.4 μm thin films of PMMA (poly-methyl methacrylate) resist show a small loss of resolution by lateral scattering of secondary electrons. The purpose of this present paper is to extend those hybrid Monte Carlo calculations to high beam voltages (100 KeV) and very thin films (0.05 μm) and compare the theoretical results with some recent experimental results published. The new results extend microstructure science and technology into the regime of "nanolithography", and demonstrate some very exciting possibilities for advanced device applications. As shown schematically in Figure 1, the resolution attainable in thin film membranes can be very high, and is analogous to the analytical resolution in STEM (scanning transmission electron microscopy) discussed by Kyser (1979).

II. MODEL FOR FAST SECONDARY ELECTRON PRODUCTION

Since the fast secondary electron production in electron resists is believed to determine the ultimate spatial resolution attainable in a lithographic process, a new Monte Carlo model for electron scattering was developed by Murata et al. (1981). The model is an extension of an earlier model developed by Kyser and Murata (1974) for simulation of electron scattering, energy loss, resist solubility, and prediction of developed images in electron beam lithography. The new model utilizes a hybrid model for primary electron scattering and energy loss with a differential cross-section for fast secondary electron production by the primary electrons along their paths. Only a brief outline of the new hybrid Monte Carlo calculation will be given. The details of the calculation are contained in the references cited.

The primary electron scattering is usually described by a screened-atom Rutherford elastic scattering cross-section, and the energy loss between elastic scattering events by the Bethe continuous energy loss equation. In the hybrid Monte Carlo model, an inelastic electron-electron scattering model for secondary electron production was incorporated as a probable alternative to elastic electron-atom scattering. The probability for elastic versus inelastic scattering is set by the relative cross-section values, and is chosen by a computer-generated random number. The cross-section of Moller was chosen to describe inelastic scattering as described in Murata et al. (1981).

Once a secondary electron is generated, its path and energy loss are simulated as if it were a primary electron, except that further discrete inelastic scattering is prohibited. Random numbers are utilized to choose scattering angles, scattering atoms, and variable step lengths in the usual manner for Monte Carlo calculations.

The concept of this hybrid Monte Carlo model is shown in Figure 2. The dashed line shows the energy-path length relationship for the Bethe continuous slowing down approximation (CSDA). In the new Monte Carlo model, the energy loss of a primary electron is calculated in a hybrid manner. The primary electron energy decreases continuously unless electron knock-on collisions occur and a fast secondary electron is produced. The trajectory of the primary electron is divided into sections when a knock-on collision occurs at energy E_1 or E_2, for example. This hybrid model for energy loss, coupled with a model for angular scattering, then produces the

LIST OF SYMBOLS

q_ℓ = Line source of electron exposure (coul/cm).
E_v = Volume density of energy deposition (eV/cm^3).
E'_v = Normalized output value from Monte Carlo calculation (keV/cell/electron).
ϵ_c = Normalized cutoff energy for secondary electron duction (dimensionless).
E = Electron energy (keV).
E_F = Minimum energy to which an electron is tracked in the Monte Carlo calculation (keV).
ΔX = Histogram cell size in Monte Carlo calculation (Å).
E' = Value of E_v/q_ℓ (eV/coul-cm^2) for a normalized equi-energy density contour.

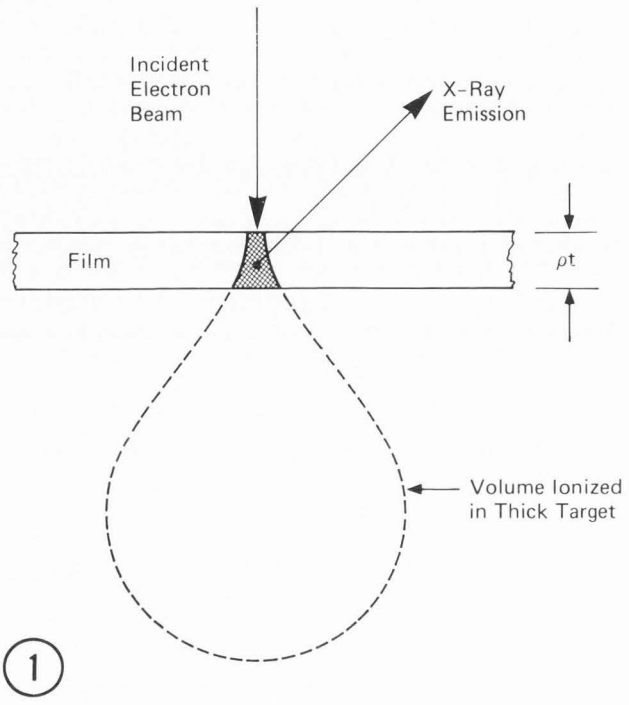

Fig. 1. A qualitative display of the volume analyzed in a foil, relative to that in a thick target.

Fig. 2. Schematic illustrations of the electron energy vs. path length curve in the hybrid Monte Carlo model.

Fig. 3. Trajectories of the primary (a) and secondary (b) electrons in a 4000 Å thin PMMA film due to 1000 electrons of 20 keV incident at the origin.

Fig. 4. The equi-energy density contours for a 4000 Å thin PMMA film with 20 keV electrons. The contour labels represent the density in normalized units of 5×10^9 eV/cm^2-electron.

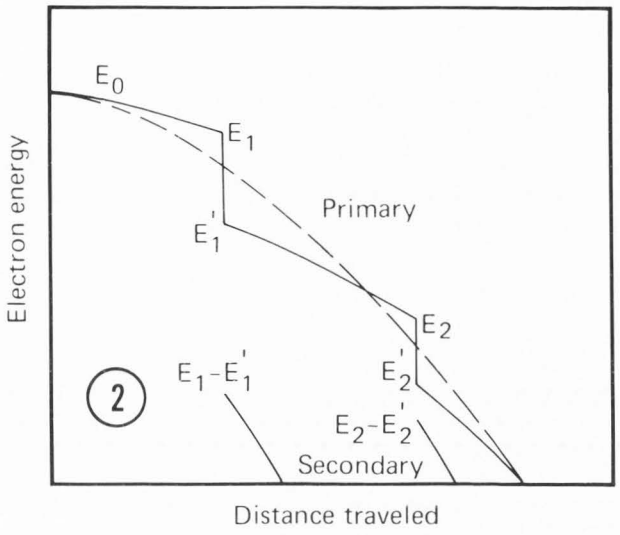

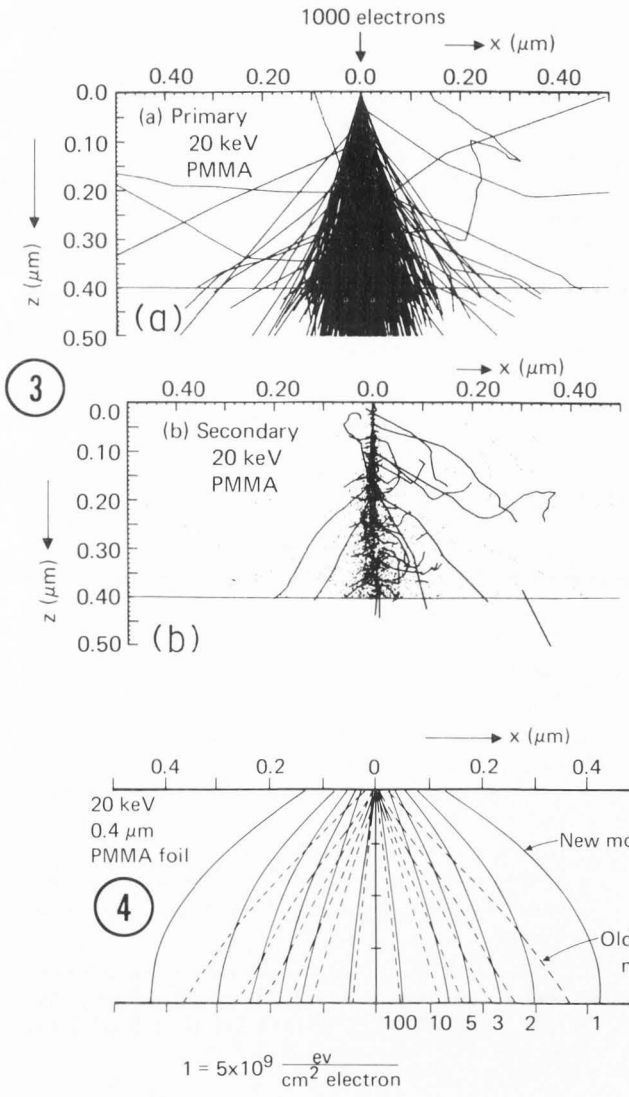

3-dimensional paths of primary and secondary electrons within the target.

As an example, the paths of 1000 primary electrons incident on a 0.4 μm foil of PMMA at 20 keV is shown in Figure 3a. The corresponding paths of the fast secondary electrons produced by these electrons is shown in Figure 3b. The elastic-scattering mean free path of 20 keV electrons is about 700 Å in PMMA. Such electrons will have several elastic scattering events within the film. Hence the primary electrons are spread out when they exit the film at the bottom in Figure 3a. The secondary electrons are generated with an energy distribution up to 10 keV, but most are generated with very small energies and hence have very short path lengths in Figure 3b. However some secondary electrons are very energetic, and many of the secondary electrons are directed almost parallel to the film plane. Such electrons can significantly limit the spatial resolution attainable in electron beam lithography.

Utilizing the electron trajectories shown in Figure 3, contours of equi-energy density E_v (eV/cm^3) deposited within the film can be calculated. These contours then represent the latent image in the resist. The results are shown in Figure 4 for the former Monte Carlo model (no explicit secondary electron production) and the new Monte Carlo model with a line source of electron exposure q_ℓ(coul/cm). For a given exposure q_ℓ, the energy density E_v can be found by multiplying the contour value (in units of eV/cm^2/electron) by q_ℓ (in units of electrons/cm) and using the scale factor indicated. Note that in Figure 4, the old model predicted a very sharp, almost conical shape for the latent image. The new model shows the quantitative effects of the fast secondary electrons on resolution, especially near the top surface of the film.

To predict the spatial resolution attainable in electron beam lithography, contours such as those shown in Figure 4 can be used in the following way. With particular solvents, the solubility of PMMA resist can be approximated by a model whereby all of the resist exposed above a particular value of E_v will dissolve, and all below that value will remain. This is called the threshold approximation, and there is no time-evolution in the model. The threshold value E_v for PMMA in a weak developer is about 1×10^{22} eV/cm^3 according to Kyser and Viswanathan (1975). If the film exposure at the top is $q_\ell = 3.2\times10^{-8}$ coul/cm, then the contour labeled 10 in Figure 4 is 1×10^{22} eV/cm^3 and this contour represents the developed image for such conditions. For this film thickness (0.4 μm) and beam voltage (20 keV) the width of the developed image changes with depth below the film surface. At a depth of 0.2 μm, which is half the film thickness, the width of the developed image is about 0.2 μm and is only about 0.3 μm at the bottom of the film. This result also shows the potential advantages of utilizing even thinner films and higher beam voltages for high-resolution electron lithography. In the next section, these film thickness and beam voltage effects on spatial resolution will be described.

With strong solvents, the threshold developer approximation will not be valid, and more sophisticated models for lithographic process simulation must be employed such as that described by Kyser and Pyle (1980). These more sophisticated models require that the resist-solvent system be characterized by systematic measurements of 1-dimensional solubility rates. The solubility rate data must then be curve-fit

with appropriate algorithms which describe the parameter-dependence of the experimental data. Only then can the 2-dimensional calculations of latent image contours be transformed into 2-dimensional (or 3) profiles of time-evolution. Nevertheless, the latent images alone can be utilized to investigate the limits of spatial resolution because the development process generally degrades resolution, and does not improve resolution. The results presented in the next section are based primarily on latent image calculations since only a limited number of resist-solvent systems have been quantitatively characterized.

III. RESULTS FOR THIN PMMA FILMS

With the new hybrid Monte Carlo model, a systematic study of beam voltage and film thickness effects on spatial resolution was made. Beam voltages of 25, 50, 75, and 100 keV were simulated and film thicknesses of 500, 1000, and 2500 Å were investigated. All of the results were obtained with the computer program and system LMS (Lithography Modeling System) described by Kyser and Pyle (1980). This software/hardware system is a powerful aid to rapidly explore process variables and also contains a very sophisticated computer terminal graphics capability for interactive, on-line calculations.

A. Electron Trajectories

The primary and corresponding secondary electron trajectories within a 1000 Å PMMA film for 25, 50, 75, and 100 keV are shown in Figures 5, 6, 7, and 8 respectively. Note that as beam voltage increases, the lateral spread of both the primary and secondary electrons decreases significantly. Also notice that the number of secondary electrons decreases with increasing voltage. In Figures 5a, 6a, 7a, and 8a the trajectories of only 1000 primary electrons were plotted. Many of the primary electrons have over-lapped trajectories on this plot resolution. In Figures 5b, 6b, 7b, and 8b the secondary trajectories generated by 10000 primary electrons were plotted in order to illustrate the effect. Within the hybrid Monte Carlo model, the following parameter values were used: $\epsilon_c = 0.001$, $E_F = 0.10$ keV, cell = 20 Å. The parameter E_F refers to the cutoff energy of the trajectory calculation, and ϵ_c is a parameter in the hybrid model.

B. Equi-Energy Density Contours

To demonstrate the dramatic effects of secondary electron production on spatial resolution, a series of calculations was made with both the old and new Monte Carlo models. Within the hybrid model, there is a parameter ϵ which describes the energy transfer $\Delta E/E$ transferred to a secondary electron by collision from a primary electron with energy E ($0.5 \geq \epsilon \geq \epsilon_c$). A normalized cutoff energy ϵ_c is also utilized, along with a minimum energy E_m, below which the knock-on production of secondary electrons is prohibited. This is necessary because the Moller cross-section for inelastic scattering is based on free-electron scattering theory, and hence is not appropriate for energy loss near to or below the ionization energy of the target atoms. Hence calculations with the old model can be made with the same hybrid Monte Carlo program by setting $\epsilon_c = 0.5$.

The equi-energy density contours within a 1000 Å PMMA film for 25, 50, 75, and 100 keV are shown in Figures 9, 10, 11, and 12 respectively. The contours in Figure 9a, 10a, 11a, and 12a were calculated with $\epsilon_c = 0.5$, and so they represent the results of the old model without inelastic scattering included explicitly. Note that these contours are very conical in shape. The relative value of each contour is labeled on the right hand side of the graph (RATO), with the higher values being the innermost contours. The numerical scale value or normalizing factor is 0.64×10^{-4} keV/electron/cell. The plot resolution is determined by the cell size of the histogram in the Monte Carlo calculation, and the statistical noise in the plot is determined by the total number of electron trajectories simulated. The histogram of the Monte Carlo calculation is formed by dividing the cross-sectional area of the film into a 2-dimensional array of parallelepipeds each with a square cross-section $(\Delta X)^2$. The energy deposited by any electron traversing the parallelepiped is calculated and the total energy deposited by all such electrons is assigned to that cell. The equi-energy density contours are then formed by connecting together all the cells which contain the same value of energy deposition. The minimum resolution in the histogram plot is then determined by the cell size ΔX. The results shown in Figure 9-12 were calculated with 500000 trajectories, and the following parameter values were used: $\epsilon_c = 0.001$ or 0.500, $E_F = 0.50$ keV, cell = 20 Å. The energy density of a particular contour can be calculated from the following equation:

$$E_v(\text{eV/cm}^3) = \frac{\text{RATO} * 10^3 * q_\ell * E'_v}{(\Delta X)^2}$$

where E'_V = output value from Monte Carlo calculation (keV/cell/electron)
q_ℓ = line source electron exposure (coul/cm)
ΔX = cell resolution of Monte Carlo histogram (Å)
RATO = relative value on graphics plot

Fig. 5. Trajectories of (a) 1000 primary electrons and (b) secondary electrons produced by 10000 primary electrons in a 1000 Å thin PMMA film for 25 keV energy.

Fig. 6. Trajectories of (a) 1000 primary electrons and (b) secondary electrons produced by 10000 primary electrons in a 1000 Å thin PMMA film for 50 keV energy.

Fig. 7. Trajectories of (a) 1000 primary electrons and (b) secondary electrons produced by 10000 primary electrons in a 1000 Å thin PMMA film for 75 keV energy.

Fig. 8. Trajectories of (a) 1000 primary electrons and (b) secondary electrons produced by 10000 primary electrons in a 1000 Å thin PMMA film for 100 keV energy.

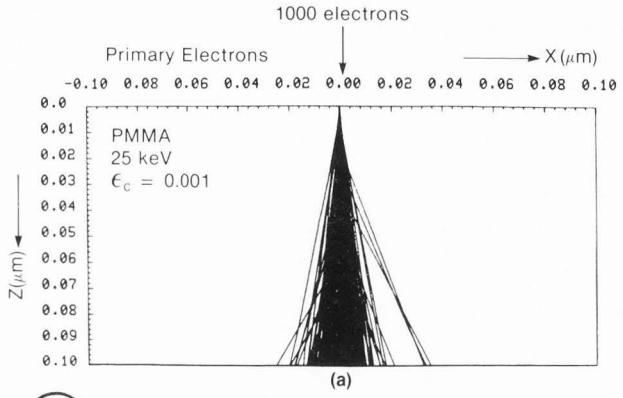

(a)

5

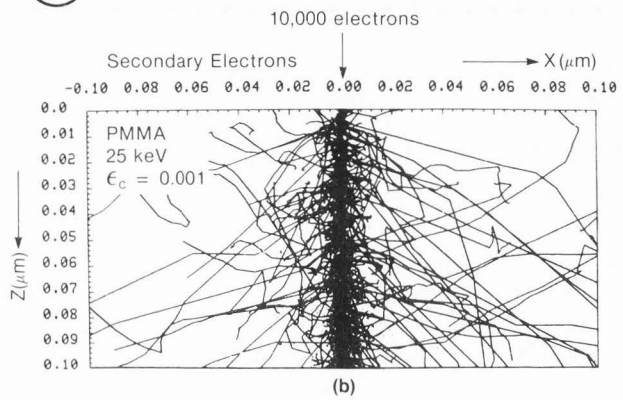

(b)

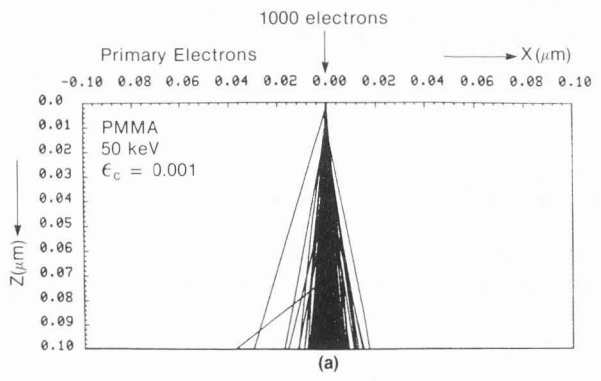

(a)

6

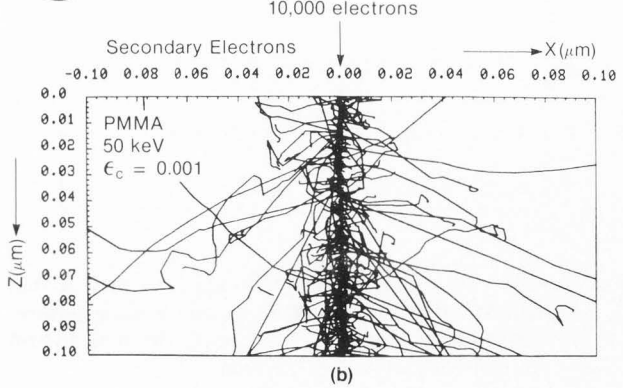

(b)

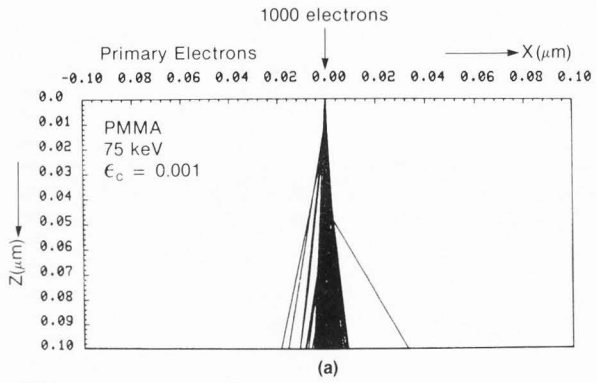

(a)

7

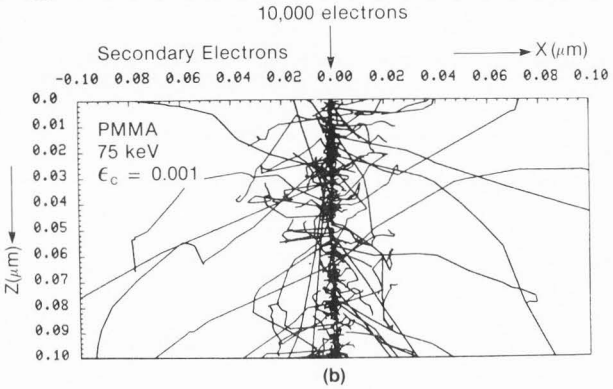

(b)

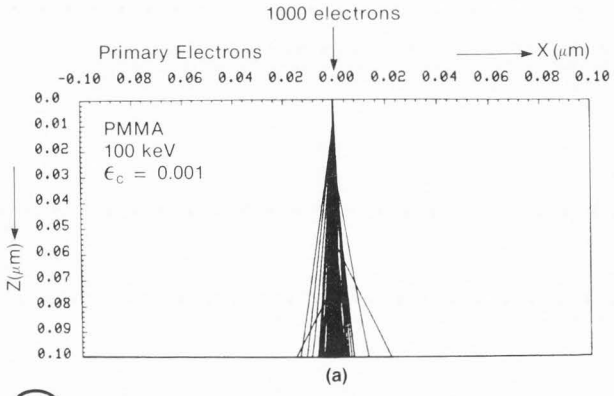

(a)

8

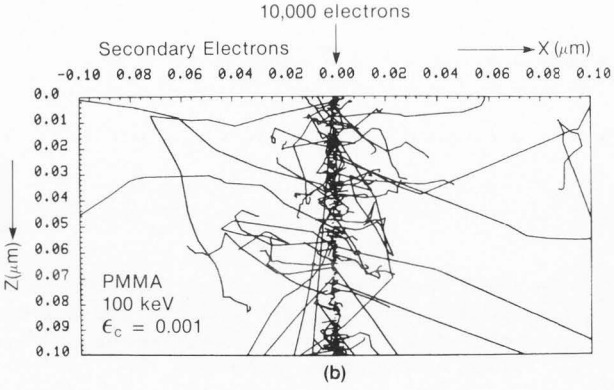

(b)

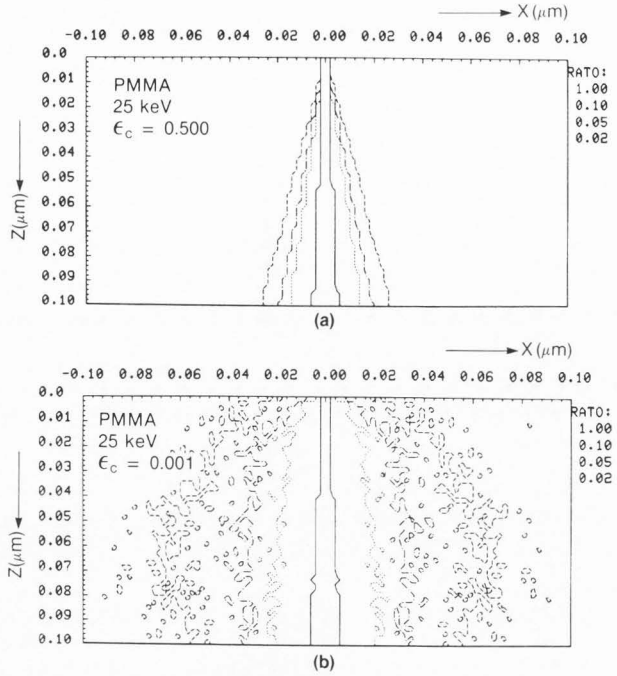

Fig. 9. The equi-energy density contours for a 1000 Å thin PMMA film with 25 keV electron beam exposure; (a) former Monte Carlo model, (b) new hybrid model with secondary electrons.

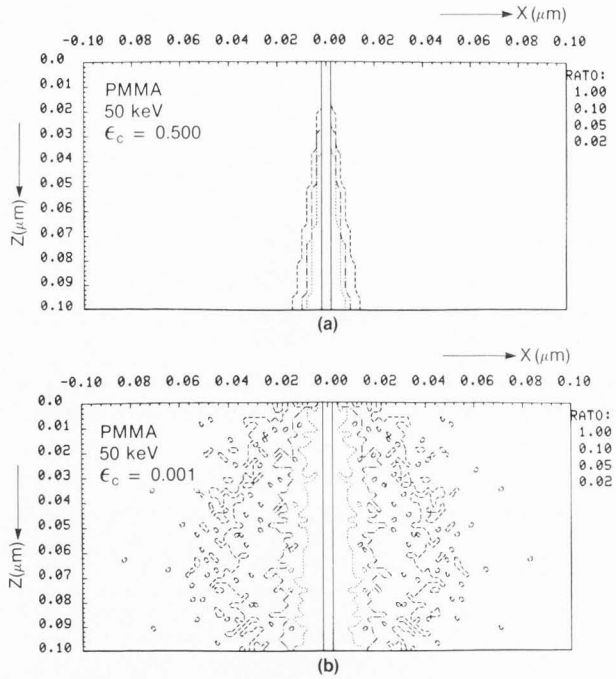

Fig. 10. The equi-energy density contours for a 1000 Å thin PMMA film with 50 keV electron beam exposure; (a) former Monte Carlo model, (b) new hybrid model with secondary electrons.

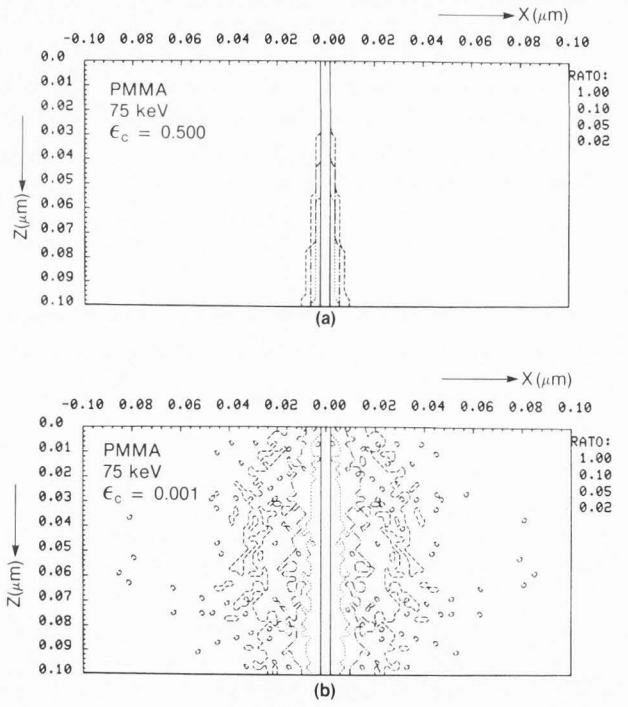

Fig. 11. The equi-energy density contours for a 1000 Å thin PMMA film with 75 keV electron beam exposure; (a) former Monte Carlo model, (b) new hybrid model with secondary electrons.

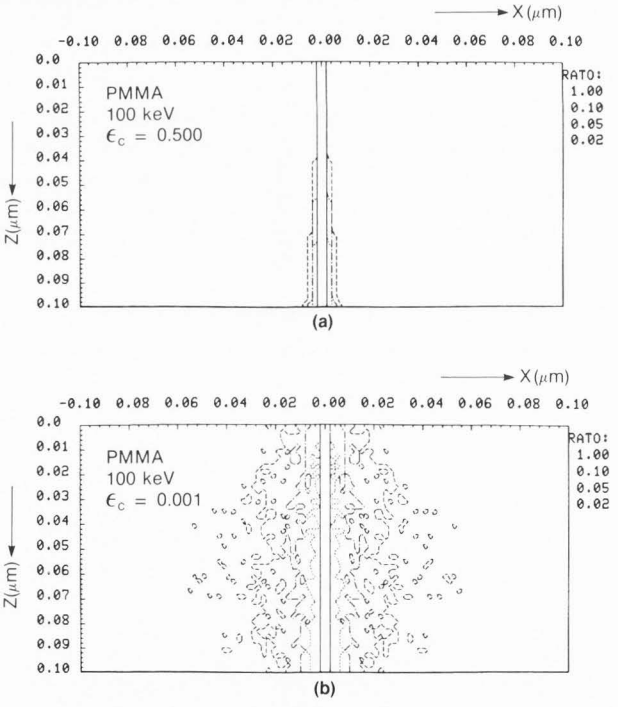

Fig. 12. The equi-energy density contours for a 1000 Å thin PMMA film with 100 keV electron beam exposure; (a) former Monte Carlo model, (b) new hybrid model with secondary electrons.

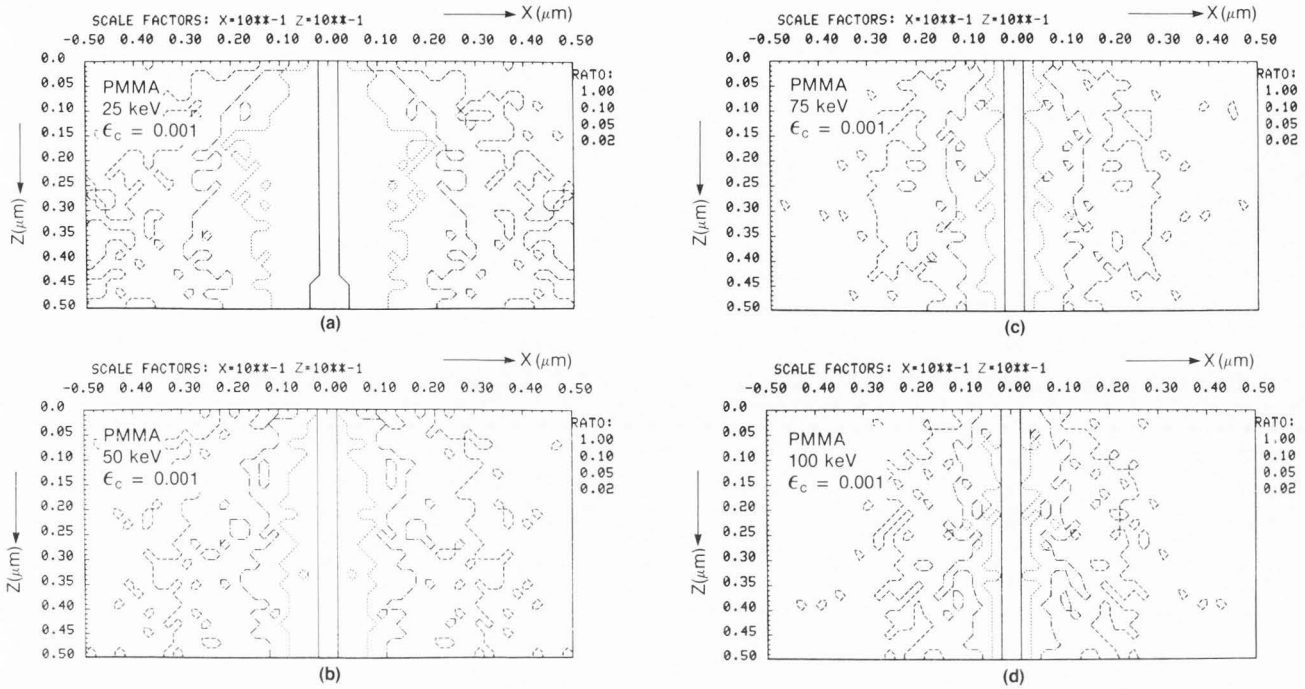

Fig. 13. The equi-energy density contours for a 500 Å thin PMMA film calculated with the new hybrid Monte Carlo model for (a) 25 keV, (b) 50 keV, (c) 75 keV, and (d) 100 keV electron beam exposure.

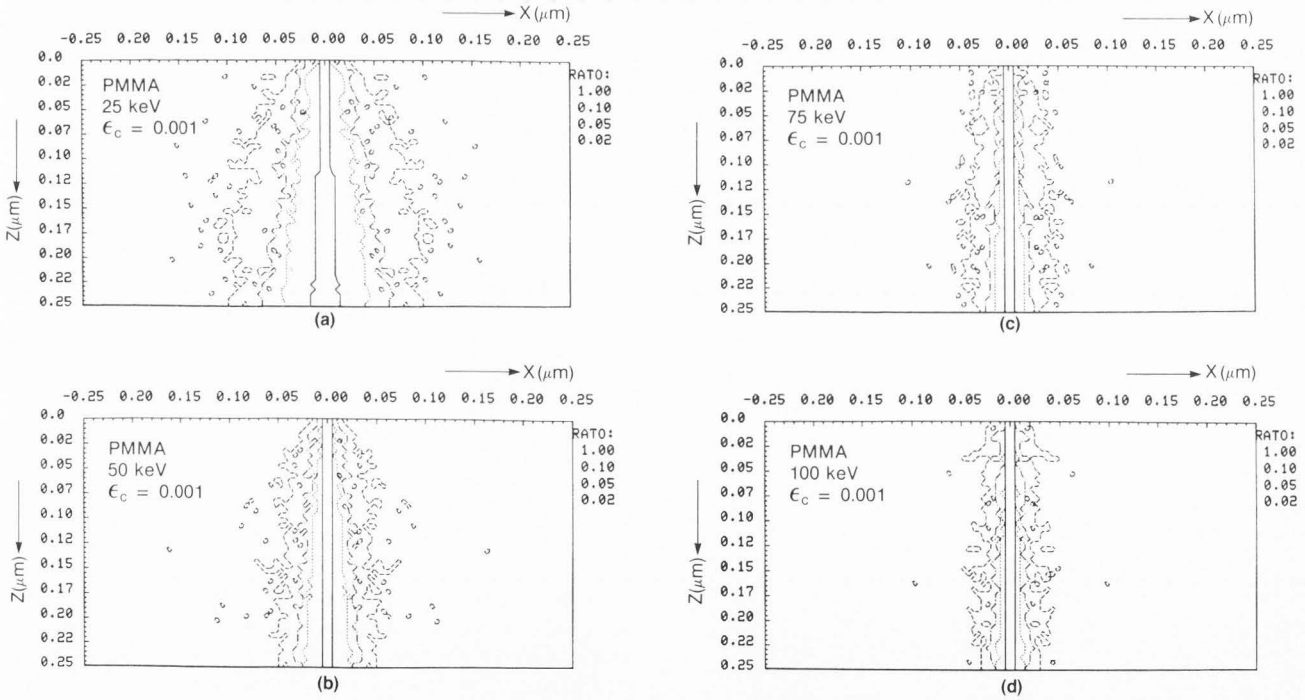

Fig. 14. The equi-energy density contours for a 2500 Å thin PMMA film calculated with the new hybrid Monte Carlo model for (a) 25 keV, (b) 50 keV, (c) 75 keV, and (d) 100 keV electron beam exposure.

The contours shown in Figures 9b, 10b, 11b, and 12b were calculated with $\epsilon_c = 0.001$, and represent the results of the hybrid model with inelastic scattering via secondary electron production included. Note that these contours are "noisier" due to the random nature of the secondary production and subsequent paths. This noise is a consequence of the statistics, even though 500000 primary electron trajectories were calculated. The noise can be improved with more trajectories or larger cell size, but only improves as $\sqrt{N}$ where N = number of trajectories. The contour can be smoothed graphically by hand, but this is not necessary for the present application. Note also that the contour narrows with increasing beam voltage.

The results shown in Figures 9-12 were for films of 1000 Å thickness. The results shown in Figures 13a, b, c, and d are for a 500 Å film at 25, 50, 75, and 100 keV respectively. Note that the scale factor on the axis is 0.1, i.e. full scale is ± 500 Å in X and 500 Å in Z. The scale factor for these plots is also 0.64×10^{-4} keV/electron/cell. The results were calculated with 500000 electrons, and the following parameters were used: $\epsilon_c = 0.001$, $E_F = 0.50$ keV, cell = 20 Å. Again, the statistical noise in the plots is determined by the value of N and the cell size in the Monte Carlo calculation. However the results obtained are sufficient to obtain some quantitative data on spatial resolution performance.

The results shown in Figures 14a, b, c, and d are for a 2500 Å film at 25, 50, 75, and 100 keV respectively. The scale factor for these plots has changed to 0.40×10^{-3} keV/electron/cell. These results were calculated with only 100000 electrons, and the following parameters were used: $\epsilon_c = 0.001$, E_F 0.50 keV, cell = 50 Å. As before, the contour narrows with increasing beam voltage.

C. Linewidths of Latent Images

The equi-energy density contours shown in Figure 9-14 and discussed in section III.B can be measured and tabulated for specific values of energy density. The most interesting cases are the thinner films, and so we have tabulated the linewidths W in Table 1 for both the 500 Å and 1000 Å films at 25, 50, 75, and 100 keV. The four values of energy density, which correspond to the four values of RATO plotted, are given in normalized units (eV/coul-cm²). This normalization value $E' = E_V/q_\ell$ and so the energy density E_v (eV/cm³) can be found easily for each particular value of line source exposure q_ℓ (coul/cm) by a simple multiplication. Some of the early experimental work on PMMA was done with weak solvents and exposure values $q_\ell = 1 \times 10^{-8}$ coul/cm. If a threshold development level of 1×10^{22} eV/cm³ is assumed, then the row in Table 1 with $E' = 1 \times 10^{30}$ eV/coul-cm² corresponds to the experimental conditions.

In Table 1, note that for a particular value of E′ the linewidth W decreases with increasing beam voltage. All of these results are for a perfect line source exposure, i.e., a negligibly small beam diameter. In practice, the electron beam diameter in a STEM instrument can approach 5 Å which approximates a line source very well. However the actual beam diameter in some experiments may not be known, and hence these results represent the ultimate limit of spatial resolution for vanishingly small beams. The highest resolution is obtained at the higher beam voltages and thinner films. Due to the cell size of 20 Å used in these Monte Carlo calculations, the plot resolution is also limited to 20 Å. Hence the minimum width contour which can be plotted is 40 Å (2 cells). The contours are forced to be symmetric by the graphics plot routine, since the left and right halves of the Monte Carlo histogram are summed together and then re-plotted as a symmetric contour after normalization.

D. Development of Latent Images

As described earlier, real resist-solvent systems do not behave exactly as a threshold development process. In most cases, the time-evolution of the developed image is important to consider. However, the solubility parameters of the system must be characterized in order to account for this effect. The lithographic simulator program LMS can also transform a latent image into a developed image, including a finite beam size. The results shown in Figures 15a, b, c, and d are for a 500 Å PMMA film exposed with a 50 Å wide Gaussian beam at 50 keV. The digital design of the incident beam is shown in Figure 15a, where the cell size is 20 Å in the Monte Carlo calculation (See also Fig. 13b for latent image of ideal line source).

With a distributed line source exposure, the electron dose must be described in terms of coul/cm². The time-evolution of the latent image with the Gaussian exposure of Fig. 15a is shown in Figure 15b at 0.25, 0.50, 0.75, and 1.00 minutes development. The development parameters are appropriate for PMMA with an unexposed solubility rate of 1 Å/sec and a contrast of 2. The electron dose is 300 μcoul/cm², and the other parameters are given in Kyser and Pyle (1980). Note that the developed profile becomes vertical and remains vertical and translates more slowly (1 Å/sec) after an initial rapid opening and translation.

If the unexposed solubility rate (RFINL) is increased from 1 to 4 Å/sec, the results are shown in Figures 15c and d. After only 0.11 minutes, the bottom of the resist is opened to about 20 Å. The time-evolution at 0.25, 0.50, 0.75, and 1.00 minutes is shown in Figure 15d. Note that here the width of the developed line is controlled primarily by the unexposed etch rate and not by the original latent usage. This points to the importance of controlling the development time and using electron resists with very small unexposed etch rates to achieve high-resolution images. This is particularly important for very thin films where the development time may reduce much of the original film thickness and hence preclude good process control and resolution. This problem may be reduced somewhat by utilizing resists which exhibit an induction time for surface etching or by multi-layer resist structures.

IV. COMPARISON OF MONTE CARLO WITH EXPERIMENTAL RESULTS

During the past 10 years, there have been a variety of experimental results published on high-resolution microlithography with focussed electron beams. The variety of methods employed include direct exposure and development of polymeric electron resist films, deposition of polymerized vacuum oil contamination, and even direct vaporization of NaCl films. In most cases, a very thin film of electron-sensitive resist has been formed on a very thin membrane substrate, and a high-resolution SEM or STEM utilized to expose the resist. After development, the resist pattern is transferred by

Table 1. Linewidths of Latent Image from Equi-Energy Density Contours

500 Å Film

E′ (eV/coul-cm²)	W (Å) 25 keV	50 keV	75 keV	100 keV
1×10^{31}	80	40	40	40
1×10^{30}	300	200	100	80
5×10^{29}	500	300	250	200
2×10^{29}	900	600	550	500

1000 Å Film

E′ (eV/coul-cm²)	W (Å) 25 keV	50 keV	75 keV	100 keV
1×10^{31}	200	40	40	40
1×10^{30}	400	300	150	100
5×10^{29}	700	400	300	250
2×10^{29}	1200	800	600	550

ion etching or by lift-off processes. The subsequent microstructure is then observed with high-resolution electron microscopy. The very thin membrane substrates are utilized both for mechanical strength and to minimize the effect of electrons which would be backscattered from thick substrates. The exposure of the thin resist film is then determined primarily by forward electron scattering (and subsequent secondary electron production).

A chronological list of experimental results is shown in Table 2. Except for the results from contamination resist writing in Broers et al. (1976) and direct film vaporation in Isaacson and Murray (1981), the results obtained in conventional resists range from 150-600 Å linewidths. The results obtained by Broers et al. (1978, 1981) and those obtained by Beaumont et al. (1981) are probably the best experiments to compare with the Monte Carlo results presented in section III.C and Table 1. In some experimental cases, the electron exposure has not been specified. However, we will assume that the threshold development for PMMA is a good approximation, with a threshold $E' = 1 \times 10^{30}$ eV/coul-cm² for the latent image. The results presented in Table 1 show a linewidth W = 200 Å in a 500 Å film, and W = 300 Å film at 50 keV beam voltage. These values of linewidth compare very well with the values observed experimentally by Broers et al. (1978, 1981) and Beaumont et al. (1981).

If we include the time-evolution of the development process, then the results shown in Figures 15b and 15d are to be compared with those observed experimentally by Broers et al. (1978, 1981).

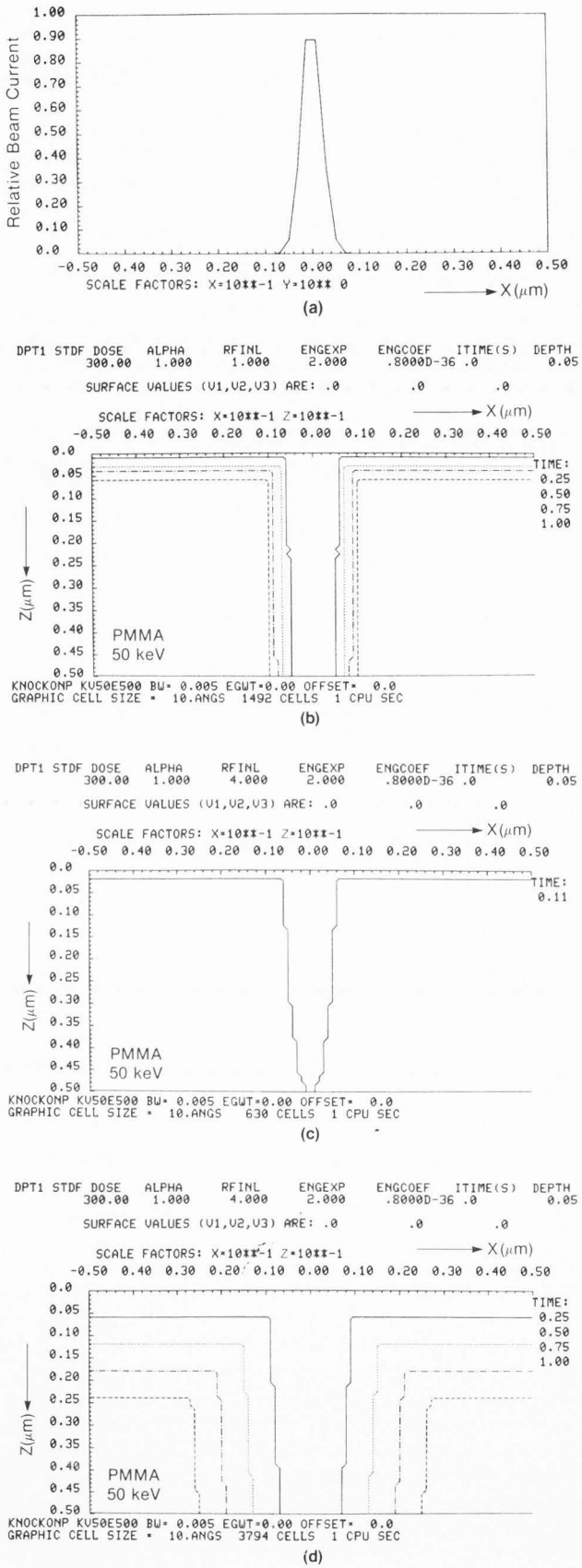

Fig. 15. Time-evolution of profile development for a 500 Å thin PMMA film exposed by a 50 Å-FWHM electron beam, 50 keV energy, and 300 μC/cm² exposure; (a) incident beam profile, (b) profiles at 0.25 minute intervals with unexposed etch rate Ro = 1 Å/sec, (c) profile at 0.11 minute with Ro = 4 Å/sec, and (d) profiles at 0.25 minute intervals with Ro = 4 Å/sec.

Table 2. Literature References on High-Resolution Electron Beam Lithography

Reference	Target Structure	Electron Beam Parameters	Development Parameters	Linewidth Resolution	Comments
Sedgwick et. al. (1972)	Thin PMMA on 1500 Å Si_3N_4	25 kV SEM $1.2x10^{-10}$ C/cm	—	600 Å single lines	600 Å Aℓ lift off
Broers et. al. (1976)	100 Å PdAu on 100 Å carbon	45 kV STEM 5 Å beam $1x10^{-6}$ C/cm	Polymerized contamination	80 Å	PdAu ion etched
Broers et. al. (1978)	1100 Å PMMA/ 225 Å PdAu on 600 Å Si_3N_4	56 kV STEM 10 Å beam 500 $\mu C/cm^2$	15-45 sec 1:3 (MIBK:IPA)	250 Å lines/gaps	"
Howard et. al. (1980)	1500 Å PMMA/ 4000 Å P(MMA/MAA) on thick Si	30 kV SEM $2\text{-}4x10^{-9}$ C/cm	5-10 sec 1:2 (cell:meth)	400 Å lines/gaps	300 Å Au lift off
Broers (1981)	300 Å PMMA on 600 Å Si_3N_4	50 kV STEM 10 Å beam 300 $\mu C/cm^2$	50 sec 1:3 (MIBK:IPA) R_0 = 4 Å/sec	225 Å lines/gaps	50 Å AuPd shadow coating
Beaumont et. al. (1981)	600 Å PMMA on 300 Å carbon	50 kV SEM 80 Å beam	30-45 sec 1:3 (MIBK:IPA)	160 Å lines 370 Å gaps	PtPd lift off
Isaacson and Murray (1981)	300 Å NaCℓ on 100 Å carbon	100 kV STEM 5 Å beam	—	15 Å lines 30 Å gaps	in-situ develop
Lee and Ahmed (1981)	500-2000 Å x-link/ 1000-3000 Å PMMA on 1000 Å Si_3N_4	50 kV STEM 10 Å beam 1000 $\mu C/cm^2$	10sec pure MIBK + 45 sec in 1:3	150 Å lines 500 Å gaps	resist only

Note that the simulated linewidth depends strongly on the unexposed solubility rate (RFINL) which is 1 Å/sec in Fig. 15b and 4 Å/sec in Fig. 15d. The minimum Gaussian beamwidth which could be simulated was 50 Å due to the digital construction of the beamshape in Figure 15a. In Broers (1981), the experimental beamwidth is estimated to be about 10 Å, and the unexposed solubility rate is estimated to be about 4 Å/sec. Hence the simulated linewidth of about 400 Å at 0.75 minutes development and 300 μcoul/cm^2 exposure in a 500 Å film (Fig. 15d) is expected to overestimate the value of about 250 Å observed experimentally in a 300 Å film with a 10 Å beam diameter. Small errors in the beamwidth, exposure, film thickness, and unexposed solubility rate measurements could explain this difference of about 150 Å in linewidth. In future comparisons of theory and experiment, it will be very important to specify with certainty these parameters. Nevertheless, there is fairly good agreement already between the Monte Carlo and experimental results obtained for conventional resist materials and development processes.

Some very interesting high-resolution lithography has been reported with thick Si substrates and multi-layer resist films. It appears that the multi-layer resist greatly reduces the intra-proximity effect due to electrons backscattered from the thick substrate. In Howard et al. (1980), 400 Å lines/gaps of 300 Å thick Au have been fabricated by a lift-off process in multi-layer resist film with only a 30 keV SEM beam. The electron beam diameter was estimated to be "several hundred angstroms". In Lee and Ahmed (1981), resist gaps of about 150 Å have been formed in multi-layer resist films on thick Si substrates with a 10 Å, 50 keV beam. These results show that high-resolution microlithography is not limited to membrane substrates. However the ultimate resolution attainable is still determined by the spatial distribution of production and energy loss by fast secondary electrons, and hence the results shown in Table 1 may also be useful for thick substrates as well. With thick substrates, multi-layer resist, and very high beam voltages, the intra-proximity and inter-proximity effects of electron scattering become very small and maybe even negligible in practice. Further calculations and experiments are necessary to establish the quantitative effects of proximity in such cases.

V. SUMMARY

A systematic, theoretical study of spatial resolution limits

in electron lithography with thin resist films has been presented. The spatial resolution is determined by the production and subsequent energy loss of fast secondary electrons generated in the film via knock-on collisions with the incident primary electrons. For an ideal line source electron beam exposure, the quantitative values of equi-energy density contours (latent image) are presented for thin films of 500 or 1000 Å and beam voltages of 25, 50, 75, and 100 keV. For a 500 Å film of PMMA exposed with 1×10^{-8} coul/cm at 100 keV, the results predict a limiting linewidth in the latent image of about 100 Å. If the exposure is decreased to 1×10^{-9} coul/cm, then a latent image linewidth of about 40 Å is predicted at 100 keV. For exposure with electron beams of finite diameter, the resolution will be worse.

When development effects are included in the simulation of linewidth, the results depend on the solubility characteristics of the resist-solvent system as well as the latent image. The results show that it is very important to utilize resists with very small unexposed solubility rates. With large unexposed solubility rates and thin films, process control is difficult. In addition, the beam diameter and electron dose need to be measured and controlled very accurately for good process control in the "nanolithography" regime of linewidths. For the published experimental results which specified the necessary data such as beam size and unexposed solubility rate, there is good agreement between the simulated and observed minimum linewidths. Further calculations and experiments are necessary to identify the most sensitive parameters in nanolithography, including the nature of proximity effects due to fast secondary electrons.

IV. ACKNOWLEDGEMENTS

The author acknowledges the helpful discussions and contributions to this work by Dr. Kenji Murata (Osaka Prefecture University, Japan) and by Mr. Richard Pyle (IBM Corp.). This work was performed while the author was a Research Staff Member at the IBM Research Laboratory.

Note added in proof:

With the exception of the polymerized contamination resist method of Broers et al. (1976) and the NaCl film evaporation method of Isaacson and Murray (1981), the *positive* resist PMMA has been exclusively used for very high resolution nanolithography experiments. Recently, Tamamura et al. (1982) published some experimental results utilizing the *negative* electron resist αM-CMS (chloromethylated poly-α-methylstyrene). The target structure was a 600 Å resist film on a 550-600 Å thin Si_3N_4 substrate. A 39 kV SEM beam with a 100 Å beam diameter and an exposure range of $1-8 \times 10^{-9}$C/cm was used. After exposure, the resist was developed sequentially in acetone (10 sec) and IPA (30 sec). With the lowest molecular weight resist material, linewidths of 230 Å on 820 Å pitch were delineated. The authors propose that the resolution in this negative resist material is a function of both the incident beam diameter, electron scattering, and also the formation of large polymer chains with electron exposure. The minimum linewidth decreased with decreasing molecular weight, but not as strongly as expected based on polymerization physics. While their observed resolution may be partially limited by the rather large beam diameter used, the results of our Monte Carlo calculations suggest that a significant increase in resolution (decrease in linewidth) can be achieved by using higher beam voltage than 39 kV (See Table 1). If the αm-CMS resist behaves as a "threshhold" material for development, then the equi-energy density curves shown in our work can be used to predict the resolution and quantitatively characterize the intrinsic sensitivity of this class of materials. The generation and transport of fast secondary electrons in such materials will still play an important role in determining the ultimate limits of spatial resolution attainable.

REFERENCES

Beaumont S, Bower P, Tamamura T and Wilkinson C. (1981). Sub-20 nm wide metal lines by E-beam exposure of thin PMMA films and liftoff. Appl. Phys. Lett. **38**, 436-439.

Broers A, Molzen W, Cuomo J and Wittels N. (1976). Electron-beam fabrication of 80 Å metal structures. J. Appl. Phys. **29**, 596-598.

Broers A, Harper J, and Molzen W. (1978). 250 Å linewidths with PMMA electron resist. Appl. Phys. Lett. **33**, 392-395.

Broers A. (1981). Resolution limits of PMMA resist for exposure with 50 kV electrons. J. Electrochem. Soc. **128**, 166-170.

Howard R, Hu E, Jackel L, Grabbe P and Tennant D. (1980). 400 Å linewidth E-beam lithography on thick substrates. Appl. Phys. Lett. **36**, 592-593.

Isaacson M and Murray A. (1981). In-situ vaporation of very low molecular weight resists using ½ nm diameter electron beams. J. Vac. Sci. Technol. **19**, 1117-1120.

Kyser D and Murata K. (1974). Monte Carlo simulation of electron beam scattering and energy loss in thin films on thick substrates, In: Proc. 6th Int. Conf. Electron and Ion Beam Science and Technology, R. Bakish (ed), Electrochemical Society, Princeton, N.J., 205-223.

Kyser D and Viswanathan N. (1975). Monte Carlo simulation of spatially distributed beams in electron beam lithography. J. Vac. Sci. Technol. **12**, 1305-1308.

Kyser D. (1979). Monte Carlo simulation in analytical electron microscopy, in: Introduction to Analytical Electron Microscopy, J. Hren, J. Goldstein and D. Joy (eds.), Plenum Press, New York, 199-221.

Kyser D and Pyle R. (1980). Computer simulation of electron beam resist profiles. IBM J. Res. Develop. **24**, 426-437.

Lee K and Ahmed H. (1981). An E-beam microfabrication system for nanolithography. J. Vac. Sci. Technol. **19**, 946-949.

Murata K, Kyser D and Ting C. (1981). Monte Carlo simulation of fast secondary electron production in electron beam resists. J. Appl. Phys. **52**, 4396-4405.

Sedgwick T, Broers A and Agule B. (1972). Novel method for fabrication of ultrafine metal lines by electron beams. J. Electrochm. Soc. **119**, 1769-1771.

Tamamura T, Suskegawa K and Sugawara S. (1982). Resolution limit of negative electron resist exposed on a thin film substrate. J. Electrochem. Soc. **129**, 1831-1835.

DISCUSSION WITH REVIEWER

R. Shimizu: Did you use the relativistic energy formulae for elastic and inelastic scattering? If not, are there serious errors in the results obtained for high energy (100 keV)?

Author: The Monte Carlo computer program used in this work is based on the original work by Murata et al. (1981). The program includes a standard relativistic correction for the *elastic* scattering mean free path. The correction is not made for the *inelastic* scattering process. However at 100 keV, $\tau = E/m_0c^2$ is about 0.2 and the relativistic correction to the *inelastic* differential cross-section and scattering angles is very small, i.e., less than 10%. Hence the non-relativistic approximation was used in *inelastic* scattering only, and does not result in a serious error at 100 keV.

R. Shimizu: The electron trajectories shown in Figure 3a give the impression that you assume all the incident primary electrons suffer initial elastic scattering at the surface. If so, does this explain the conical shapes of the equi-energy density contours shown in Figures 9a, 10a, 11a, and 12a?

Author: The Monte Carlo calculations in this paper do *not* assume that the incident electrons are initially scattered at the surface. After penetration into the target, a primary electron undergoes either an initial elastic or inelastic scattering event. The value of this initial scattering depth below the surface is exponentially distributed in the standard manner of modern Monte Carlo calculations. This behavior is not very apparent in Figure 3a because of the overlapping trajectory plots which are not resolved in this computer-generated plot, especially along the axis of electron incidence. However, real-time observation of such trajectory plots on a storage CRT shows the actual distribution in depth of the first scattering event. Such plotting is very fascinating to observe, and is also very educational.

R. Shimizu: Have you calculated the energy distribution of transmitted electrons with the hybrid Monte Carlo program? Although comparison with experimental results is difficult due to limited data, a comparison with results obtained from other Monte Carlo work may be useful for quantitative discussion.

Author: A discussion on the results obtained with this new hybrid Monte Carlo program for transmitted electron energy distribution is contained in Murata et al. (1981). The hybrid model certainly improves the quantitative results obtained, relative to an earlier non-hybrid model with elastic scattering only, when compared with some experimental data in the literature. While the results obtained from a direct, more fundamental approach to Monte Carlo simulation of electron scattering may be more accurate in specific targets, the hybrid Monte Carlo approach utilized in the present work may be more practical and applicable to general targets.

R. Shimizu: How many random numbers were used in the simulation of 500000 trajectories? Is there a problem with re-occurrence of a computer-generated random number?

Author: It is difficult to know the exact total of random numbers used because of probability in hybrid scattering. At 100 keV, there is less than 1 scattering per electron in a 0.1 μm PMMA film. If there are 8 random numbers/event, then there is a maximum of 4×10^6 random numbers needed for 500000 trajectories. This large number is comparable to the re-occurrence period of the random number algorithm used in this work. However, this effect can be eliminated when necessary by using several "lists" of random numbers and using each "list" for only a fraction of the total trajectories. The individual "lists" of random numbers are generated by using different "trigger" numbers in the computer algorithm. The random numbers on the "list" are generated sequentially, and only on request by the main Monte Carlo program for use in subsequent calculations.